ACS APPLIED NANO MATERIALS

www.acsanm.org Article

Hybrid Grating-Hole Nanostructures Produced by Spatiotemporal Modulation of Femtosecond Lasers: Implications for Near-Field Enhancement

Zhen Zhao and Jianjun Yang*

Cite This: ACS Appl. Nano Mater. 2022, 5, 9576−9583 Read Online

ABSTRACT: Here, we report a method or one-step generation of peculiar hybrid grating-hole nanostructures on Fe-based metallic surfaces upon irradiation with spatiotemporally modulated femtosecond lasers, i.e., orthogonal linear polarizations of time-delayed double laser beams are manipulated into a tightly spatial energy distribution by optical diffraction. It is surprisingly found that the induced surface structures not only present the highly uniform appearance but also consist of two different geometric components: the ablation subwavelength grating pattern with a spatial period of 707 nm and the well-distributed nanohole arrays on the ridge areas. Remarkably, both the grating length and the nanohole numbers can be controlled by varying the laser energy fluence. Theoretical analyses reveal that the formation of these structures can be attributed to the surface plasmon excitation and the light scattering of finite-length microstructures. Moreover, further simulation and experimental results clearly demonstrate the near-field enhancement effect of such laser-induced structures, which provides a promising way toward on-demand manipulation of the light response and detection in metadevices.

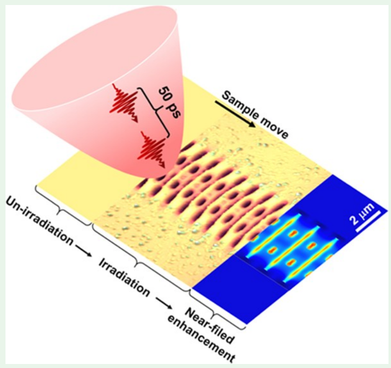

KEYWORDS: *femtosecond laser, metallic glass, hybrid nanostructures, light scattering of finite-length microstructures, near-field enhancement*

1. INTRODUCTION

Over recent years, micro- or nanostructures and their based devices have attracted considerable interests because of the fundamental significance and the remarkable applications, such as THz radiation enhancement,[1] extraordinary optical transmission,[2] light manipulation,[3] and optical waveguides.[4] Currently, the well-defined high precision structure is usually produced by some traditional methods, including ion-beam etching,[5] nanoskiving,[6] electron-beam lithography,[7] and oblique angle codeposition,[2] however, they are likely to exhibit a low throughput because of the rigid requirements in costly devices, complex procedures, and large time consuming.

By comparison, the extensive study in multidisciplinary fields has proved that lasers can act as an important tool for the high precision machining and processing. Especially, the arising femtosecond laser-induced periodic surface structures (LIPSSs) are widely regarded as a new convenient way to construct the subwavelength periodic gratings on metals,[8−10] semiconductors,[11,12] and dielectrics.[13,14] With the help of exploiting the physical effects in the laser−material interaction, the formation of intriguing nanostructures, such as the dot matrix,[15] spindle chains,[16] and triangular arrays,[17] has ever been reported. As for the material of metallic glass, the LIPSS formation has been identified with the enhanced distribution regularity,[10,18] which is benefited from the special atom arrangements with the short-range order but long-range disorder. Of course, besides the influence of material properties, both the geometric profile and the arrangement regularity of laser-induced structures are closely related to the field distribution of the incident laser. For example, Öktem et al. reported the extraordinary regular LIPSS on thin metal films using the high-repetition-rate femtosecond laser, where the laser focusing spot was emphasized to shrink into a range less than 10 laser wavelengths so that all points within the beam spot can contribute to the mutual electromagnetic field and avoid the independent creation of structures.[9] Namely, the spatial coherence of the excited surface waves can be preserved more easily on a small irradiation area, thus facilitating the birth of the regularly controlled structures. However, a comprehensive understanding of the physics involved is still missing.

In this letter, we investigate the controllable formation of the anomalous hybrid grating-hole structures on Fe-based metallic glass upon irradiation of two time-delayed femtosecond laser

Received: April 25, 2022
Accepted: June 3, 2022
Published: June 16, 2022

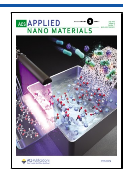

https://doi.org/10.1021/acsanm.2c01787
ACS Appl. Nano Mater. 2022, 5, 9576−9583

beams with a spatially modified pulse energy distribution to show the tight uniform and controllable energy fluence. The obtained grating component exhibits the subwavelength period of Λ = 707 nm, with orientation perpendicular to the polarization direction of the prior incident laser, while the achieved nanoscale hole component displays well-defined array profiles on the ridge areas, and remarkably, the hole numbers are well controlled by varying the laser energy fluence. The theoretical analyses based on the surface plasmon excitation and the light scattering of the finite-length microstructures provide the simulation results to match well the experimental observations. In particular, the laser-induced hybrid nanostructures can be considered as a platform for choosing the near-field enhancement distribution, which is demonstrated by the simulation and experimental results.

2. MATERIALS AND METHODS

Figure 1 presents a schematic diagram of the experiment setup, in which the linearly polarized femtosecond laser pulses are generated by a Ti:sapphire femtosecond laser amplifier (Spectra Physics HP-Spitfire 50), with a central wavelength of 800 nm and a pulse duration of 40 fs. Its output at a repetition rate of 1 kHz results in 1 ms (Δt = 1 ms) temporal spacing between two neighboring pulses. For the purpose of correlating ultrafast dynamics between two adjacent laser−material interactions, we designed a Michelson interferometer-like configuration to acquire the picosecond temporal delay of laser subpulses. Namely, each pulse output from the laser system was divided into two identical parts in the time domain, and then, they propagated along two different arms in the space domain, wherein the adjustable optical path via the delay-line movement can be used to precisely change the traveling time of the laser subpulses. Moreover, a quarter-wave plate was inserted in one of the optical arms to modulate the two subpulses into orthogonal linear polarizations, and the neutral attenuators were employed within both arms to control the pulse energy. Afterward, the two spatially separated laser subpulses were collected into the overlapping collinear propagation by a beam splitter and finally obtained a coaxial beam focusing through an objective lens (Nikon, 4×, NA = 0.1). With the help of such an optical design, the single-beam irradiation of 1 kHz repetition rate femtosecond laser pulses can be easily obtained by blocking the one optical arm.

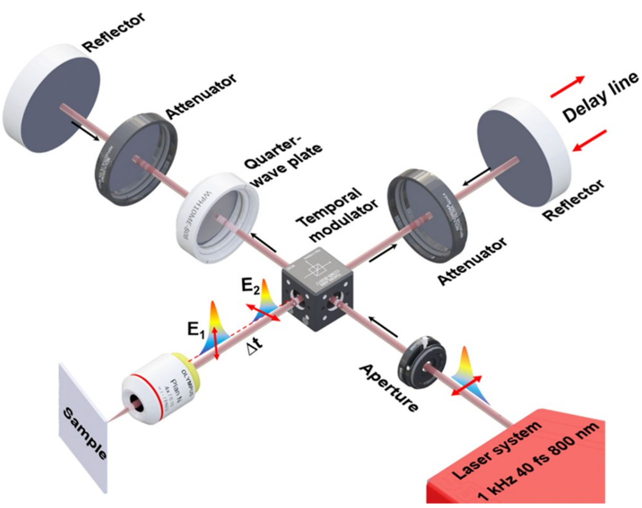

Figure 1. Schematic diagram of the experimental setup for generating the peculiar hybrid grating-hole nanostructures on the surface of Fe-based metal glass upon irradiation of the space−time modulation of femtosecond laser pulses (red double arrows represent the direction of the laser polarization; red single arrow for the delay-line movement; and black single arrow for the direction of the laser propagation).

In our experiments, a 40 μm thick foil of Fe-based metal glass ($Fe_{85}Si_9B_6$) was adopted as a sample material in consideration of its superior physical and chemical properties, including high plasticity,[19] charming stabilization,[20] and excellent thermal and magnetic properties.[21] And it was fixed on a computer-controlled three-dimensional translation stage (Newport, ESP301) for the laser striking at normal incidence. To avoid the severe laser ablation behaviors, we placed the sample surface 430 μm away before the laser focus, leading to the laser spot diameter of about 60 μm. All of the experiments were carried out in ambient air by a line-scribing method with a scanning speed of 1 mm/s, resulting in approximately 120 laser pulses partially overlapped within a beam spot area. The calculation of laser peak fluence is based on the formula $F = 2E_0/\pi w_z^2$, with E_0 being the pulse energy and w_z the spot radius on the sample surface.[22,23] After the laser processing, the surface morphologies were examined by both a scanning electron microscope (SEM, HITACHI, S-4800) and an atomic force microscope (AFM, BRUKER, Multimode 8).

It is worth mentioning that before spatially dividing the laser pulse into two parts, a 6 mm diameter hard circular aperture was placed in the laser path to restrict the large beam size, and its optical diffraction can consequently modulate the spatial distribution of the laser intensity,[24] as shown in Figure 2a. The calculation of the optical field energy distributions is based on using Seelight software, where the incident laser wavelength and the diameter of a circular beam modulator are set as 800 nm and 6 mm, respectively. The focal length of the optical lens is 45 mm, and the monitored plane is set 430 μm in front of the focus. In contrast to the condition without using the hard aperture, the center part of the diffracted laser spot (marked by the purple stripe region within the intensity distribution curve in Figure 2a) can drastically reduce the effect area of the laser action, when the pulse energy is properly adjusted above the damage threshold F_s of the material. The use of the hard aperture tends to concentrate the

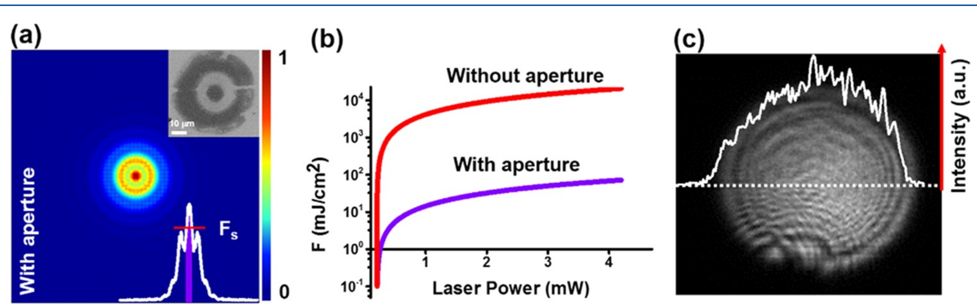

Figure 2. (a) Normalized laser diffraction patterns on the sample surface when using the hard aperture in the optical path, where the white curve represents the modified spatial distribution of the laser intensity and the upper-right picture for a measured SEM image of the laser-irradiated surface. (b) Calculated variations of the energy fluence as a function of the incident laser power for two cases with and without using the hard aperture. (c) Measured charge-coupled device (CCD) image of the laser intensity distribution without using the hard aperture and the derived curve of the spatial laser intensity distribution.

https://doi.org/10.1021/acsanm.2c01787
ACS Appl. Nano Mater. 2022, 5, 9576−9583

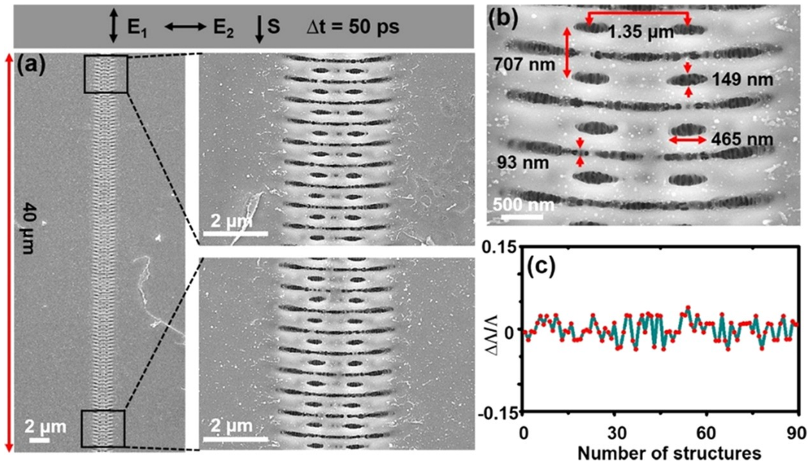

Figure 3. Formation of the hybrid grating-hole structures on the Fe-based metallic surface irradiated by the spatiotemporal modulation of femtosecond lasers, where two femtosecond laser beams have a time delay of Δt = 50 ps with orthogonal linear polarizations, and the energy fluences of the prior and delayed incident laser subpulses are F_1 = 62 mJ/cm^2 and F_2 = 45 mJ/cm^2, respectively. (a) SEM images of the laser-induced hybrid nanostructure patterns. Here, E_1 and E_2 represent the directions of two laser polarizations, and S for the sample scanning direction. (b) Higher resolution SEM image. The red arrows mark the structure geometric profiles. (c) Measured statistical fractional variations of the induced grating period.

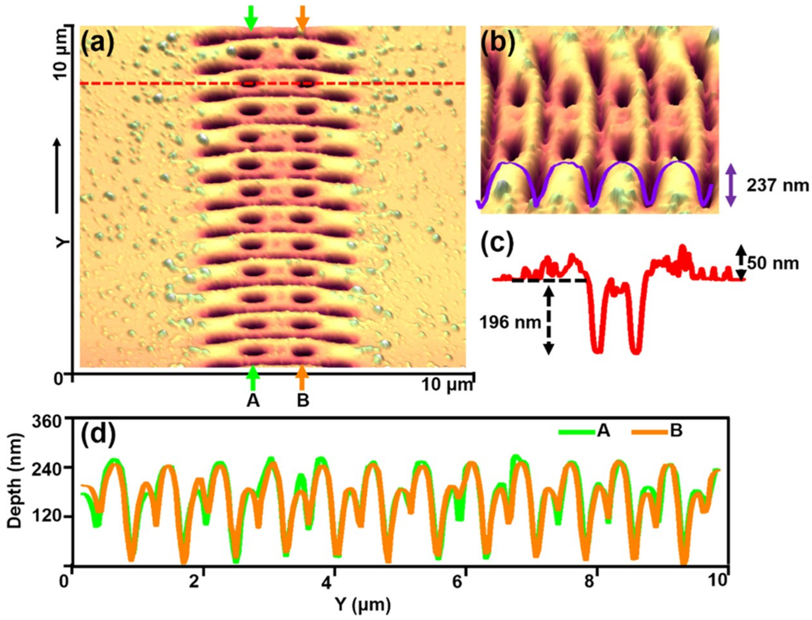

Figure 4. (a, b) AFM measurements of the hybrid grating-hole nanostructures induced by the femtosecond lasers. (c, d) Measured cross-sectional curves for two positions marked in panel (a) with different colors.

laser energy into an evidently narrow region (about 7 μm in diameter). Although such a tight localization of the laser energy can be achieved by direct focusing, our experimental method makes the manipulation of the laser fluence become more convenient with the help of large diffraction patterns.

This idea is confirmed by the simulation of the laser-power-dependent energy fluence for two situations: with and without using the hard aperture, as shown in Figure 2b. It is clear that in the case of direct focusing, the achieved energy fluences tend to vary dramatically by four orders of magnitude, especially at the small laser power values, and much larger energy fluences are exhibited at the slight improvement of the laser power values. In the case of the hard aperture, the optical diffraction effect can significantly decrease the gradient of the energy fluence variation with the laser power values, thus leading to the effective control of the laser fluence within a small range. Moreover, we also measured the laser intensity distribution by a CCD for the situation without the hard aperture, as illustrated in Figure 2c, where the obvious energy jitters are seen within the laser beam spot. On the contrary, in the case of the hard aperture, the energy jitters become almost disappeared due to the diffraction effect, leading to the spatially smooth and uniform laser intensity distribution.

3. EXPERIMENTAL RESULTS AND DISCUSSION

Figure 3 shows the experimental observations on the sample surface upon irradiation of spatiotemporally modulated femtosecond lasers, where the two laser subpulses linearly polarized in orthogonal directions possess a time delay of Δt = 50 ps (here, the horizontally polarized laser beam E_2 is temporally delayed), associated with the energy fluences of F_1 = 62 mJ/cm^2 and F_2 = 45 mJ/cm^2. The scanning velocity of the sample is V = 1 mm/s, along the direction parallel to the polarization direction of the prior laser pulse. As shown in the SEM images, the surface structures present the uniform and peculiar morphology. In specific, apart from the component of periodic subwavelength grating structures, as reported by many previous researche studies,[10−12] two elliptical nanoholes can be observed on each ridge surface. Moreover, along the direction of the laser scanning, the spatial alignment of the nanoholes seems to be coherently locked into the regular profile. Therefore, such complex laser-induced patterns can earn the appellation "hybrid grating-hole nanostructures". The corresponding higher resolution SEM image, as shown in Figure 3b, reveals that the grating component has a spatial period of approximately Λ = 707 nm, with a groove width of about W = 93 nm between two adjacent ridges. On the surface of each grating ridge, two elliptical nanoholes, having the major and minor lengths of approximately 465 and 149 nm, respectively, are spaced by 1.35 μm.

It should be mentioned that our achieved hybrid surface structures are different from the previous reports on Si wafers,[25,26] which can be represented by the evidently coherent arrangement of the nanohole arrays and the distinguishable periodic ablation grooves. Remarkably, such peculiar uniform hybrid nanostructures can be induced by the femtosecond laser in one-step processing. In addition, by collecting the statistical measurements (a total number of 90 measured data) from the SEM images, we obtained the fractional variations of the grating period over the large range, with a value of $\Delta\Lambda/\Lambda < 0.05$, which indicates a high degree of the arrangement regularity for the femtosecond laser-induced surface structures.

Moreover, the hyperfine ripples having a period of tens of micrometers can be observed on the bottom of the grooves and nanoholes, with orientation perpendicular to the grating direction. The formation of such structures is believed due to the nonuniform distribution of the surface energy followed by thermal melting and resolidification. During these processes, the strong temperature gradients can trigger the occurrence of thermocapillary instabilities, and the consequent surface tension-driven melt flow leads to the hyperfine ripple formation.[27,28]

To facilitate the understanding of the structure formation, we further obtained the elaborate morphology information through AFM measurements, as shown in Figure 4a. And, the variation of the geometric profiles for the grating component is shown in Figure 4b, with a modulation depth of about D = 237 nm. The measurement result in Figure 4c shows the nanohole depth of approximately 196 nm. The observation of the bulging morphology beside the nanoholes indicates that the thermal melting and expansion of the material may be taken place during the grating structure formation. In addition, the uniform distribution features of the surface structures are also quantitatively evaluated by the AFM measurements, as shown in Figure 4d, where the measured curves at two different portions (marked by the arrows of A and B in Figure 4a) seem to be almost consistent, indicating the well-defined capability of such hybrid nanostructure formation.

For the strong absorbing metallic materials, many previous reports have already proved that the morphology of femtosecond laser-induced structures can be effectively modulated by the energy fluence.[29,30] With the curiosity of how the formation of hybrid grating-hole nanostructures is varied with laser parameters, we carried out the experiments by only changing the energy fluence of the delayed laser subpulse, and the corresponding results are shown in Figure 5. In addition to the distinctive regular appearance, another interesting point for laser-induced structures is that both the number of nanoholes and the transversal length of the grating component are modulated. In other words, when the energy fluence of the delayed laser subpulse decreased to F_2 = 35 mJ/cm^2, the generated nanoholes were seen to transfer into the single-array distribution, and the transversal length of the grating component is decreased to L = 2.5 μm, as shown in Figure 5a. As a matter of fact, if the energy fluence of the delayed laser subpulse continued to reduce, no structures can be formed on the sample surface. For the larger laser energy fluence of F_2 = 52 mJ/cm^2, the transversal length of the grating component was extended to L = 4.5 μm, associated with three nanoholes on the ridge surface, as shown in Figure 5b.

Noticeably, as the energy fluence of the delayed laser subpulse was larger than F_2 = 60 mJ/cm^2, the above hybrid nanostructures disappeared and tended to evolve into the periodic grating structures

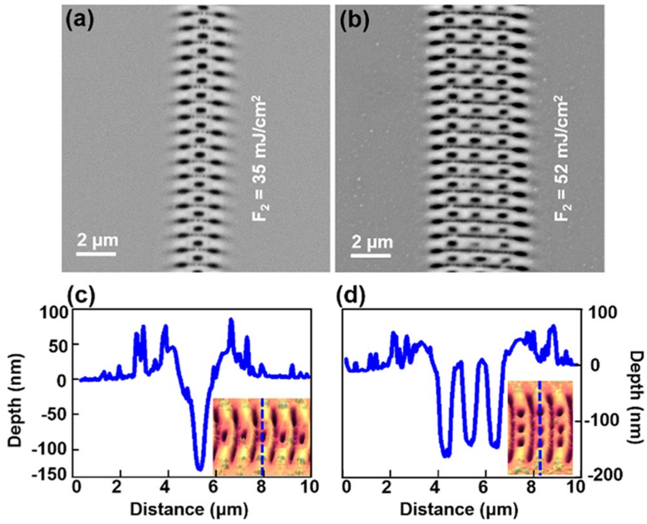

Figure 5. SEM and AFM images of the hybrid grating-hole nanostructures by varying the energy fluences of the delayed laser subpulse. (a, c) for F_2 = 35 mJ/cm^2; (b, d) for F_2 = 52 mJ/cm^2. The extracted cross-sectional curves from the AFM images (marked by the blue dotted lines).

with a transversal length more than L = 20 μm, which implied a certain degree of physical links between the nanohole formation and the grating component. Moreover, the topography of the hybrid nanostructures including one or three nanohole arrays is also measured by AFM, as shown in Figure 5c,d, which shows the structure depths slightly reducing to D = 140 and 161 nm, respectively. All in all, the aforementioned results provide direct evidence for the effective control of the hybrid grating-hole nanostructures by varying the energy fluence of the delayed laser subpulse.

In the pioneering research studies,[31,32] some authors pointed out in both experiment and theory the physical importance of the laser-induced grating structures, wherein the scattering electromagnetic wave is generated from the existent surface morphology and subsequently interferes with the incident laser to redistribute the optical field, resulting in the grating splitting phenomenon. Similarly, in our experiments, the development of the hybrid nanostructures can be comprehended as a result of two successive physical processes during the laser−material interaction. To be specific, the grating component is first developed by the interference of the prior incident laser subpulse with its surface plasmon−polariton (SPP) excitation on the material surface. This is because not only the grating orientation is perpendicular to the direction of the prior laser polarization but also the measured spatial grating period approximates the calculated SPP wavelength of λ_{spp} = 733 nm.

Once the periodic subwavelength grating structures are formed on the sample surface, the optical energy of the subsequent laser irradiation will be affected for redistribution. To deeply reveal this kind of modulation, we simulated the spatial distributions of the incident laser energy on the periodically grooved surface using the three-dimensional finite-difference time-domain (3D-FDTD) method. As shown in Figure 6a, the grooves were set to have rectangle profiles with a width of W = 100 nm, depth of D = 250 nm, and spatial period of Λ = 700 nm but different transversal lengths of L = 2.5, 3.5, and 4.5 μm, respectively. It should be mentioned that for the sample surface irradiated by the double-pulsed femtosecond lasers with orthogonal linear polarizations and nonidentical energy fluences, the laser-induced periodic grating structures are predominated by the laser pulse of the relatively higher energy fluence.[33] In particular, the significance of the delayed incident laser pulse (E_2) is considered to keep the physical properties of the material surface, i.e., the measured optical refractive index of $n = 3.06 + i\ 3.95$ for the material is employed to simulate the local field enhancements, because the latter

https://doi.org/10.1021/acsanm.2c01787
ACS Appl. Nano Mater. 2022, 5, 9576−9583

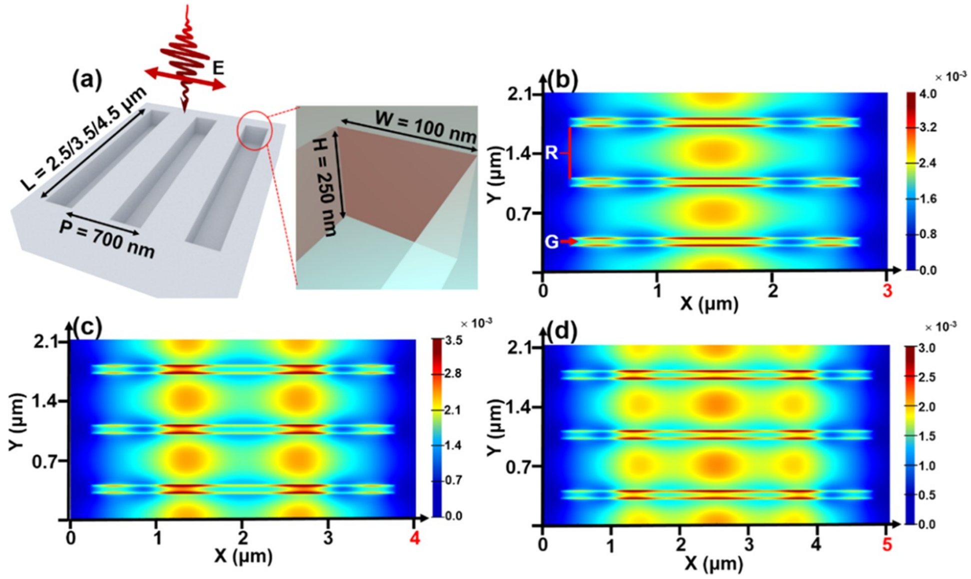

Figure 6. (a) Schematic diagram of the periodic grooves on the metallic glass for the simulations. (b−d) Calculated optical energy distributions for the grating structure (W = 100 nm, H = 250 nm, and Λ = 700 nm) with different transversal lengths of L = 2.5, 3.5, and 4.5 μm, respectively, when the laser irradiation is linearly polarized perpendicular to the groove orientation (R: ridge surface and G: groove region).

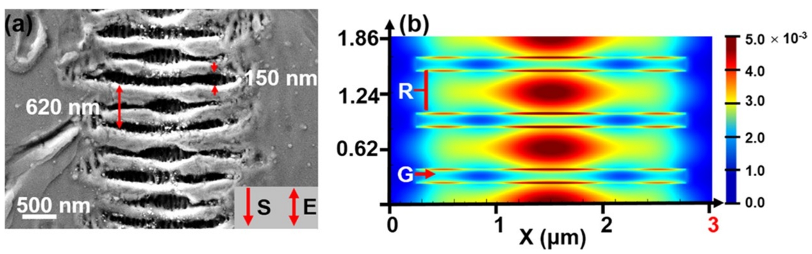

Figure 7. (a) SEM image of the structure formation under irradiation of the single-beam femtosecond laser pulses, where the laser energy fluence is F = 129 mJ/cm^2. (b) Simulation result of the laser field distribution for the existing grating structure (L = 2.5 μm, W = 150 nm, H = 250 nm, and Λ = 620 nm) but with the modulated optical refractive index of n = 1.92 + i 2.49.

can effectively suppress the phase explosion of the material surface triggered by the prior laser pulse.[34] Therefore, a Gaussian light (with the wavelength of 800 nm) was introduced at normal incidence, with the linear polarization perpendicular to the groove orientation, being similar to the prior laser pulses (E_1). The boundaries of the simulation region were truncated by the perfectly matched layers, while the boundaries in the direction perpendicular to the groove were set as the periodic conditions.

Figure 6b−d illustrates the FDTD simulation results for the grating structures with variable transversal lengths. For the case of L = 2.5 μm, only one spot of the local field enhancement is seen to take place on the center part of each grating ridge surface, and its subsequent material removal corresponds to the hybrid structure of single-array nanohole formation. It is interesting that when the transversal length of the grating component is extended to L = 3.5 μm, there are two spots of the local field enhancement emerging on the grating ridge surface, and their subsequent interaction with the material will result in the hybrid structures of two-array nanohole formation. As expected, for the grating design with the larger transversal length of L = 4.5 μm, the simulation result demonstrates three spots of the local field enhancement happening on the grating ridge surface, which corresponds to the hybrid structures of three-array nanohole formation.

Briefly, the transversal length of the grating plays a crucial role in the final formation of the hybrid structure profiles. Of course, to clarify the effect of other geometric parameters on the optical field redistribution, we also calculated with different grating depths and the ridge widths when L = 2.5 μm. For grating depths less than D = 50 nm, the simulation results exhibit no spots of the local field enhancement on the ridge surface. However, by increasing the grating depth to D = 100 nm, two spots of the local field enhancement appear on the bilateral edges of the ridge surface, and they are seen to coalesce into one spot localization at the center of the ridge surface when the grating depth is varied within a range of D = 200−250 nm. Similarly, for groove widths larger than W = 150 nm, the single spot of the local field enhancement will split into two parts with the distributions close to the bilateral edges of the ridge surface.

For the formation of a single nanohole array, when the time delay of double laser pulses changed within a range of Δt = 20−60 ps, the hybrid grating-hole structures can be still observed. To further demonstrate the structure formation at the larger time delays, we here employed the single-beam femtosecond laser irradiation with 1 kHz repetition rate, during which the time delay of two adjacent pulses is increased up to Δt = 1 ms. We observed the grating splitting from the period of approximately Λ = 620 nm rather than the formation of the above hybrid structure, as shown in Figure 7a. Here, the employed laser peak fluence of the single-beam experiment is F = 129 mJ/cm^2, slightly larger than the sum of the previously used double pulses, the reason for which may be the lower ablation threshold of the material driven by double-pulsed laser irradiation.[35] And we employed only the laser pulse E_1 for the structure formation while blocking the delayed laser pulse E_2 to reach the target. This phenomenon can be understood by the FDTD simulation with the optical refractive index having a small value of n = 1.92 + i 2.49, where the local field enhancements not only show a stronger intensity but also have a larger transversal extension on the ridge surface, thus leading to the splitting of the grating structures via the material removal, as shown in Figure 7(b). Here, the reduced optical refractive index can be

https://doi.org/10.1021/acsanm.2c01787
ACS Appl. Nano Mater. 2022, 5, 9576−9583

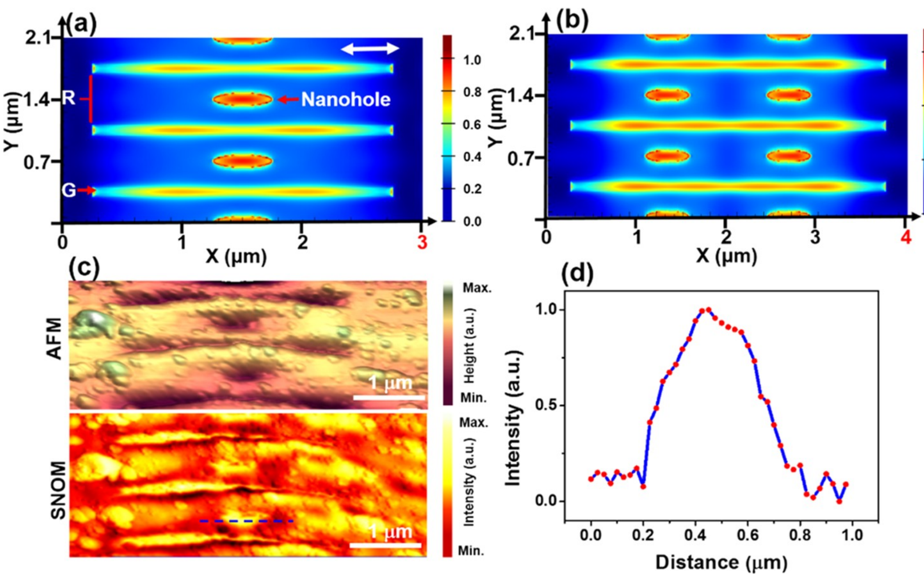

Figure 8. Calculated results of the near-field enhancement for the hybrid structures with either the single-array (a) or double-array nanohole formation (b). The white double arrows represent the direction of the incident light polarization. The structure parameter includes the grating components L = 2.5 μm, W = 150 nm, H = 250 nm, and Λ = 700 nm, and the elliptical nanohole components with a major axis length of 500 nm, the minor axis length of 150 nm, and H = 250 nm. (c) Measured AFM and SNOM images of the hybrid structures with the single-array nanohole. (d) Extracted intensity curve of the near-field intensity distribution from the position marked by the blue dotted line in panel (c).

attributed to the air−nanoparticle composite interface because the phase explosion-based ablation mechanism causes the violent ejection of materials from the surface into small clusters.[36] However, the employment of two time-delayed laser subpulses can effectively suppress the phase explosion and convert the material removal into the liquid layer spallation,[34,37] thus nearly preserving the optical properties of the original air−material interface. In other words, it is the different physical processes of the light−material interaction that modify the optical refractive index of the material surface to consequently result in the distinct experimental observations between double-pulsed and single-beam femtosecond laser irradiations.

Now, an open question is naturally raised: what about the potential of such uniform hybrid grating-hole structures? Recently, tailoring of the electromagnetic near-field properties is considerably interesting because of the wide applications in detection, photovoltaics, and sensing. However, the adopted microstructures are generally obtained by complex techniques such as ion-beam etching, e-beam lithography, and metal evaporation. Figure 8a,b demonstrates the calculations of the near-field distribution for our fabricated hybrid structures with the single-array and double-array nanohole formation, respectively, under the light illumination of 633 nm wavelength. The results unambiguously show that the enhanced near-field distributions become pronounced in the nanoholes. Figure 8c illustrates the practical mapping of the near-field distribution on the hybrid structure surface with the single-array nanohole formation, using an aperture-type near-field scanning optical microscope (SNOM), and the observation of hot spots at the nanohole positions is consistent with our simulations. The retrieved data of the near-field intensity across the nanohole is shown in Figure 8d, which confirms the effect of near-field enhancement triggered by the nanoholes.

4. CONCLUSIONS

In summary, we have employed the spatiotemporal modulation of femtosecond laser irradiation to successfully fabricate the highly uniform distribution of the hybrid grating-hole nanostructures on the surface of Fe-based metal glass. In the time domain, the incident femtosecond laser is divided into double subpulse beams with orthogonal linear polarizations and the time delay of Δt = 50 ps; while in the space domain, their laser spots are modified via the hard circular aperture to show some characteristics of the tight spatial restriction, smooth intensity distribution, and easily tunable energy fluence. The available surface structures not only show a highly uniform distribution but also exhibit two different components: one is the ablative subwavelength periodic grating with orientation perpendicular to the polarization direction of the prior incident laser subpulse and the other is the nanohole arrays coherently locked on the grating ridge surfaces. More importantly, the excellent control of such hybrid structures can be easily carried out by adjusting the energy fluence of the delayed laser subpulse.

The deep insights into the underlying mechanisms suggested that the formation of the peculiar hybrid grating-hole nanostructures is originated from two physical processes: at first, the development of the periodic grating profiles based on the SPP excitation of the prior incident laser subpulse and, subsequently, the generation of discrete local field enhancement spots due to the energy scattering of subsequent laser pulses by the finite length of the grating component. The simulation results agree with the experimental observations to confirm the validity of our theory. Such hybrid surface structures fabricated within one-step processing can be considered as a platform for supporting the modulation of the near-field distribution, which may be helpful in the future design of the optical data recording, sensors, and biomedical applications.

■ ASSOCIATED CONTENT

Supporting Information

The Supporting Information is available free of charge at https://pubs.acs.org/doi/10.1021/acsanm.2c01787.

Simulation details and the formation of the periodic grating (PDF)

https://doi.org/10.1021/acsanm.2c01787
ACS Appl. Nano Mater. 2022, 5, 9576−9583

■ AUTHOR INFORMATION

Corresponding Author

Jianjun Yang – *GPL Photonics Lab, Changchun Institute of Optics, Fine Mechanics and Physics, Chinese Academy of Sciences, Changchun 130033, China*; orcid.org/0000-0002-6703-4403; Email: jjyang@ciomp.ac.cn

Author

Zhen Zhao – *GPL Photonics Lab, Changchun Institute of Optics, Fine Mechanics and Physics, Chinese Academy of Sciences, Changchun 130033, China; Center of Materials Science and Optoelectronics Engineering, University of Chinese Academy of Sciences, Beijing 100049, China*

Complete contact information is available at: https://pubs.acs.org/10.1021/acsanm.2c01787

Author Contributions

The manuscript was written through contributions of all authors.

Notes

The authors declare no competing financial interest.

■ ACKNOWLEDGMENTS

This research was financially supported by the K.C. Wong Education Foundation (GJTD-2018-08) and the National Natural Science Foundation of China (Grant No. 91750205). The authors greatly appreciate Prof. Shaojuan Li for the help in the SNOM measurement.

■ REFERENCES

(1) Zhang, P.; Zhang, Y.; Tang, M. Enhanced THz Smith-Purcell radiation based on the grating grooves with holes array. *Opt. Express* **2017**, *25*, 10901–10910.
(2) Wang, Y.; Chong, H.; Zhang, Z.; Zhao, Y. Large-area fabrication of complex nanohole arrays with highly tunable plasmonic properties. *ACS Appl. Mater. Interfaces* **2020**, *12*, 37435–37443.
(3) Wang, S.; Dong, H.; Sun, F.; Zhang, W.; Liang, Y.; Tian, L.; Wang, P.; Yin, X.; Li, G. Large-area fabrication of highly tunable hybrid plasmonic-photonic structures based on colloidal lithography and a photo reconfigurable polymer. *Adv. Opt. Mater.* **2019**, *7*, No. 1900483.
(4) Liu, H.; Zhu, S. Coupled magnetic resonator optical waveguides. *Laser Photonics Rev.* **2013**, *7*, 882–900.
(5) Desbiolles, B. X. E.; Bertsch, A.; Renaud, P. Ion beam etching redeposition for 3D multimaterial nanostructure manufacturing. *Microsyst. Nanoeng.* **2019**, *5*, No. 11.
(6) Xu, Q.; Rioux, R.; Whitesides, G. Fabrication of complex metallic nanostructures by nanoskiving. *ACS Nano* **2007**, *1*, 215–227.
(7) Yoon, G.; Kim, I.; So, S.; Mun, J.; Kim, M.; Rho, J. Fabrication of three-dimensional suspended, interlayered and hierarchical nanostructures by accuracy-improved electron beam lithography overlay. *Sci. Rep.* **2017**, *7*, No. 6668.
(8) Xue, L.; Yang, J.; Yang, Y.; Wang, Y.; Zhu, X. Creation of periodic subwavelength ripples on tungsten surface by ultra-short laser pulses. *Appl. Phys. A* **2012**, *109*, 357–365.
(9) Öktem, B.; Pavlov, I.; Ilday, S.; Kalaycıoğlu, H.; Rybak, A.; Yavaş, S.; Erdoğan, M.; Ilday, F. Nonlinear laser lithography for indefinitely large area nanostructuring with femtosecond pulses. *Nat. Photonics* **2013**, *7*, 897–901.
(10) Lei, Y.; Yang, J.; Cong, C.; Guo, C. Fabrication of homogenous subwavelength grating structures on metallic glass using double-pulsed femtosecond lasers. *Opt. Lasers Eng.* **2020**, *134*, No. 106273.
(11) Huang, M.; Zhao, F.; Cheng, Y.; Xu, N.; Xu, Z. Origin of laser-induced near-subwavelength ripples: interference between surface plasmons and incident laser. *ACS Nano* **2009**, *3*, 4062–4070.
(12) Wang, L.; Chen, Q.; Cao, X.; Buividas, R.; Wang, X.; Juodkazis, S.; Sun, H. Plasmonic nano-printing: large-area nanoscale energy deposition for efficient surface texturing. *Light: Sci. Appl.* **2017**, *6*, No. e17112.
(13) Shimotsuma, Y.; Kazansky, P.; Qiu, J.; Hirao, K. Self-organized nanogratings in glass irradiated by ultrashort light pulses. *Phys. Rev. Lett.* **2003**, *91*, No. 247405.
(14) Zou, T.; Zhao, B.; Xin, W.; Wang, Y.; Wang, B.; Zheng, X.; Xie, H.; Zhang, Z.; Yang, J.; Guo, C. High-speed femtosecond laser plasmonic lithography and reduction of graphene oxide for anisotropic photo response. *Light: Sci. Appl.* **2020**, *9*, No. 69.
(15) Cong, J.; Yang, J.; Zhao, B.; Xu, X. Fabricating subwavelength dot-matrix surface structures of Molybdenum by transient correlated actions of two-color femtosecond laser beams. *Opt. Express* **2015**, *23*, 5357–5367.
(16) Zhao, Z.; Zhao, B.; Lei, Y.; Yang, J.; Guo, C. Laser-induced regular nanostructure chains within microgrooves of Fe-based metallic glass. *Appl. Surf. Sci.* **2020**, *529*, No. 147156.
(17) Zheng, X.; Zhao, B.; Yang, J.; Lei, Y.; Zou, T.; Guo, C. Noncollinear excitation of surface plasmons for triangular structure formation on Cr surfaces by femtosecond lasers. *Appl. Surf. Sci.* **2020**, *507*, No. 144932.
(18) Zhang, W.; Cheng, G.; Hui, X.; Feng, Q. Abnormal ripple patterns with enhanced regularity and continuity in a bulk metallic glass induced by femtosecond laser irradiation. *Appl. Phys. A* **2014**, *115*, 1451–1455.
(19) Yao, K. F.; Zhang, C. Fe-based bulk metallic glass with high plasticity. *Appl. Phys. Lett.* **2007**, *90*, No. 061901.
(20) Inoue, A. Stabilization of metallic supercooled liquid and bulk amorphous alloys. *Acta Mater.* **2000**, *48*, 279–306.
(21) Inoue, A.; Shinohara, Y.; Jin, S. Thermal and magnetic properties of bulk Fe-based glassy alloys prepared by copper mold casting. *Mater. Trans., JIM* **1995**, *36*, 1427–1433.
(22) Wang, S.; Jiang, L.; Han, W.; Liu, W.; Hu, J.; Wang, S.; Lu, Y. Controllable formation of laser-induced periodic surface structures on ZnO film by temporally shaped femtosecond laser scanning. *Opt. Lett.* **2020**, *45*, 2411–2414.
(23) Krüger, J.; Kautek, W. Ultrashort pulse laser interaction with dielectrics and polymers. In *Polymers and Light*; Springer, 2004; Vol. *168*, pp 247–290.
(24) Dumitru, G.; Romano, V.; Weber, H.; Sentis, M.; Marine, W. Femtosecond ablation of ultrahard materials. *Appl. Phys. A: Mater. Sci. Process.* **2002**, *74*, 729–739.
(25) Zhang, C.-Y.; Yao, J.; Liu, H.; Dai, Q.; Wu, L.; Lan, S.; Trofimov, V.; Lysak, T. Colorizing silicon surface with regular nanohole arrays induced by femtosecond laser pulses. *Opt. Lett.* **2012**, *37*, 1106–1108.
(26) Yuan, D. Q.; Wu, Q.; Xu, J.; et al. Periodic nanohole array structure induced on a silicon surface by direct writing with a femtosecond laser. *J. Opt. Technol.* **2015**, *82*, 353–356.
(27) Kirichenko, N. A.; Barmina, E. V.; Shafeev, G. A. Theoretical and experimental investigation of the formation of high spatial frequency periodic structures on metal surfaces irradiated by ultrashort laser pulses. *Phys. Wave Phenom.* **2018**, *26*, 264–273.
(28) Rudenko, A.; Abou-Saleh, A.; Pigeon, F.; Mauclair, C.; Garrelie, F.; Stoian, R.; Colombier, J. P. High-frequency periodic patterns driven by non-radiative fields coupled with Marangoni convection instabilities on laser-excited metal surfaces. *Acta Mater.* **2020**, *194*, 93–105.
(29) Moradi, S.; Kamal, S.; Englezos, P.; Savvas, G. Femtosecond laser irradiation of metallic surfaces: effects of laser parameters on superhydrophobicity. *Nanotechnology* **2013**, *24*, No. 415302.
(30) Yu, X.; Zhang, Q.; Qi, D.; Tang, S.; Dai, S.; Zhang, P.; Xu, Y.; Shen, X. Femtosecond laser-induced large area of periodic structures on chalcogenide glass via twice laser direct-writing scanning process. *Opt. Laser Technol.* **2019**, *124*, No. 105977.
(31) Song, J.; Tao, W.; Gong, M.; Ye, J.; Dai, Y.; Ma, G.; Qiu, J. The three-level ripples induced by femtosecond laser on a 6H-SiC single

crystal and the formation mechanism. *Appl. Phys. A* **2016**, *122*, No. 450.
(32) Yao, J.-W.; Zhang, C.; Liu, H.; et al. High spatial frequency periodic structures induced on metal surface by femtosecond laser pulses. *Opt. Express* **2012**, *20*, 905−911.
(33) Fraggelakis, F.; Stratakis, E.; Loukakos, P. A. Control of periodic surface structures on Silicon by combined temporal and polarization shaping of femtosecond laser pulses. *Appl. Surf. Sci.* **2018**, *444*, 154−160.
(34) Li, T.; Guo, Y.; Mizutani, M.; Xu, S. Surface smoothing of bulk metallic glasses by femtosecond laser double-pulse irradiation. *Surf. Coat. Tech.* **2021**, *408*, No. 126803.
(35) Gaudiuso, C.; Giannuzzi, G.; Volpe, A.; Lugarà, P.; Choquet, I.; Ancona, A. Incubation during laser ablation with bursts of femtosecond pulses with picosecond delays. *Opt. Express* **2018**, *26*, 3801−3813.
(36) Lim, H. U.; Kanga, J.; Guo, C.; Hwanga, T. Manipulation of multiple periodic surface structures on metals induced by femtosecond lasers. *Appl. Surf. Sci.* **2018**, *454*, 327−333.
(37) Tsibidis, G. D.; Barberoglou, M.; Loukakos, P.; Stratakis, E.; Fotakis, C. Dynamics of ripple formation on silicon surfaces by ultrashort laser pulses in subablation conditions. *Phys. Rev. B* **2012**, *86*, No. 115316.

https://doi.org/10.1021/acsanm.2c01787
ACS Appl. Nano Mater. 2022, 5, 9576−9583